ACS OMEGA

Open Access

http://pubs.acs.org/journal/acsodf

Article

Cage-Based 3D Tetrahexagonal Boron Nitride Crystal with Excellent Terahertz Light Absorption

Kashif Hussain, Suling Shen,* Muhammad Abbas, Madhavamoorthi Suresh, Bin Chen, Ying Teng, YunHong Jiang, Qiang Liu,* Qiang Sun, and Zhengbiao Ouyang

Cite This: *ACS Omega* 2024, 9, 44487−44493

Read Online

ACCESS | Metrics & More | Article Recommendations | Supporting Information

ABSTRACT: In recent findings, a new classification of 1D and 2D tetrahexagonal boron nitrides (*th*-BN) consisting of square and hexagonal rings has been documented. These materials exhibit impressive properties such as the tunable band gap, strong optical absorption, suitable sign-tunable Poisson's ratio, and high ideal strength, making them promising for applications in nano- and opto-electronic industries. Stimulated by these studies, we have designed a cage-based three-dimensional tetrahexagonal boron nitride (3D *th*-B_6N_6) structure, which demonstrates excellent thermal, dynamic, and mechanical stability, including exceptional cohesive and formation energies of 6.66 and −0.93 eV per atom. Unlike direct band gap 1D and 2D tetrahexagonal boron nitride semiconductors, the proposed 3D tetrahexagonal boron nitride exhibits an insulating nature, with a wide indirect band gap of 6.175 eV at the HSE06 level. Moreover, in contrast to the unequal chemical bonding and ultraviolet optical absorption observed in the 2D *th*-BN sheet, all B and N atoms form a fully sp^3-hybridized bonded 3D *th*-B_6N_6 structure, with excellent terahertz light absorption in the range of 0.3−10 THz. Notably, it also exhibits a Debye temperature of 1304.55 K and substantial phonon inelastic scattering. Our study introduces the BN family with novel properties and potential applications.

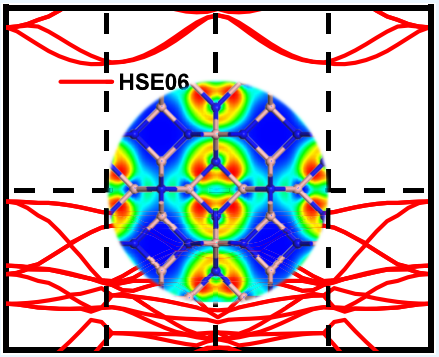

1. INTRODUCTION

Similar to tetrahexagonal BN cages,[1] a 2D tetrahexagonal BN (*th*-BN) sheet has been reported recently,[2] showing sizable indirect band gap and sign-tunable Poisson ratio, which is different from the conventional hexagonal BN (*h*-BN) sheet consisting of hexagons. Moreover, under hydrogenation and strain, the tetrahexagonal BN sheet shows some unique properties of auxetic nature, band gap transition, exotic electronic behavior, high career mobility, high ideal strength, and highly direction-dependent and tunable optical absorption spectrum, suggesting its applications in optoelectronic devices.[2] However, there is a scarcity of studies reporting the Terahertz (THz) optical properties of the 1D and 2D tetrahexagonal boron nitride materials.

It is also encouraging that the THz optical properties of several grades of *h*-BN have been investigated, so we can benefit from their technological applications.[3,4] More specifically, at 2 THz, the PBN grade can show an absorption coefficient of 0.85 cm^{-1} and a refractive index of 2.11, indicating its applications in many walks of life.[4] Therefore, it is highly desirable to find better THz-assisted BN materials due to their exciting applications.

When going beyond the 0D tetrahexagonal BN cage and 2D tetrahexagonal BN sheet, we study the 3D tetrahexagonal BN solid here. The structure model is based on the recently synthesized 2Sr@B_6C_6,[5] where Sr atoms are encapsulated in B−C cages composed of squares and hexagons. When Sr atoms are removed, the resulting tetrahexagonal BC structure (3D-B_6C_6) is found to be metallic with Pugh's ratio of 2.24, low Vickers hardness of 8.66 GPa, and universal anisotropy index of 2.62.[6] When B is further replaced with C, the 3D tetrahexcarbon is formed, which is found to be brittle with a high Vickers hardness of 53.28 GPa, and it carries a semiconducting nature with an indirect band gap of 3.92 eV at the HSE06 level and exhibits anisotropic elasticity, suitable UV−Vis light absorption, and notable phonon inelastic scattering.[7] Here, we replace C in 3D-B_6C_6 with N to form a 3D tetrahexagonal BN solid and carry out its systematic study.

2. COMPUTATIONAL DETAILS

In this study, the calculations are based on the density functional theory[8] executed in the Vienna *ab initio* simulation package (VASP).[9] The projector-augmented wave scheme[10] is implemented to study the interactions between ion cores and valance electrons with an energy cutoff of 500 eV. The

Received: July 2, 2024
Revised: October 1, 2024
Accepted: October 8, 2024
Published: October 23, 2024

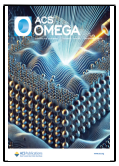

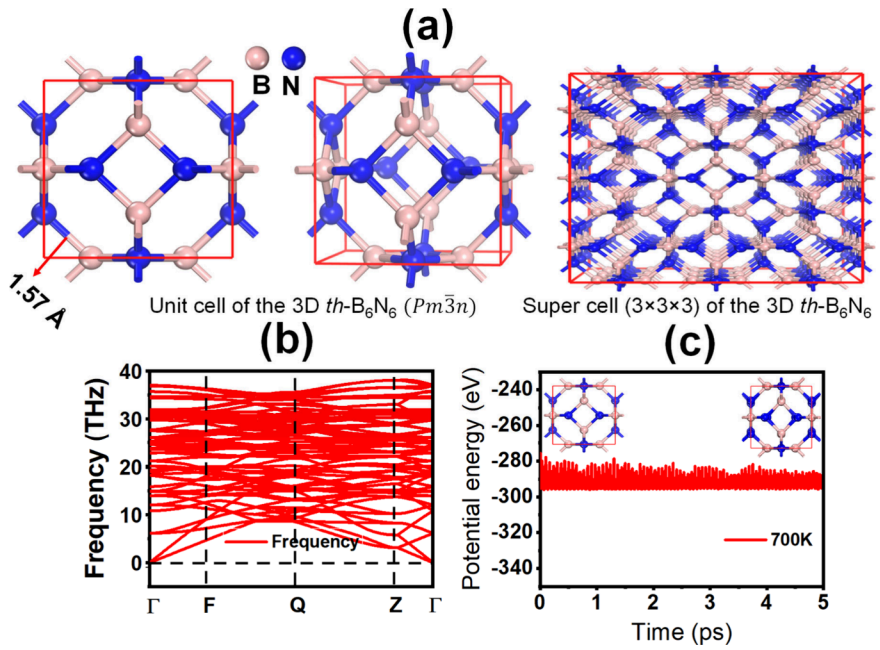

Figure 1. (a) Schematic views of the porous 3D *th*-B_6N_6 crystal, (b) phonon spectrum, and (c) energy fluctuation with time in AIMD simulations at 700 K.

Table 1. Space Group (S.G.), Lattice Constant (L.C.) (in Å), Electronic Band Gap with PBE (E_g^{PBE}) and HSE06 (E_g^{HSE06}) Functionals (in eV), Bond Type, Bond Distance d_{B-N} (in Å), and Cohesive Energy E_{coh} (in eV per atom) of the 3D *th*-B_6N_6 in Comparison with 2D Tetrahexagonal BN (*th*-BN), 2D 4H-*th*-BN-4H, and 3D Monoclinic B_5N_5 (*m*-B_5N_5), Hexagonal BN (*h*-BN), Wurtzite (*wz*-BN), and Zinc-Blende (*zb*-BN), Respectively[a]

Structure	S.G.	L.C.	E_g^{PBE}	E_g^{HSE06}	Type	d_{B-N}	E_{coh}	Ref.
3D *th*-B_6N_6	$Pm\bar{3}n$	a = 4.442, α = 90°	4.545	6.175	Indirect	1.570	6.66	This work
2D *th*-BN	*Pccm*	a = 4.560, b = 6.203	3.24	4.49	Indirect	1.583	6.13	2
2D 4H-*th*-BN-4H	-	a = 4.503, b = 6.178	3.99	5.15	Direct	1.597	6.13	2
3D *m*-B_5N_5	*Pm*	a = 6.143, b = 2.562, c = 4.145, β = 74.74°	-	4.629	-	-	-	20
3D *h*-BN	Bulk	a = 2.511, c/a = 2.66	4.47*	-	Indirect	1.450	8.825	16
3D *wz*-BN	Bulk	a = 2.542, c/a = 1.63	5.726*	-	Indirect	1.561	8.725	16
3D *zb*-BN	Bulk	a = 2.561	4.50*	-	Indirect	1.568	8.745	16

[a]The results with * are calculated with GGA-PW91.

Perdew–Burke–Ernzerhof (PBE) functional estimates the exchange-correlation energy.[11] The hybrid Heyd–Scuseria–Ernzerhof (HSE06) functional is also applied to get more accurate electronic band structure calculations.[12] The geometry is fully optimized with the convergence criterion of total energy (10^{-6} eV) and force (10^{-4} eV/Å). The mesh size of 11 × 11 × 11 is adopted for sampling the *k*-points in the first Brillouin zone (BZ) using the Monkhorst–Pack scheme.[13] Also, the dynamic and thermal stabilities are checked using the phonon calculations[14] and *ab initio* molecular dynamics (AIMD) simulations.[15]

3. RESULTS AND DISCUSSION

3.1. Geometry. By substituting C with N atoms in the 3D-B_6C_6,[6] we design the structure of the 3D *th*-B_6N_6, and the resulting optimized structure is a caged-based tetrahexagonal boron nitride (similar to the 3D tetrahexcarbon[7]), as shown in Figure 1(a), unfolding the presence of sp^3-hybridized B–N bonds in the 3D *th*-B_6N_6. Its unit cell contains 6 atoms of each boron and nitrogen, along with cubic (O_{3h}^1) symmetry (space group: $Pm\bar{3}n$), lattice constants of $a = b = c$ = 4.442 Å, angles of $\alpha = \beta = \gamma$ = 90 °, volume of V = 87.63 Å^3, and mass density of ρ = 2.821 g cm^{-3}. Also, the B–N bond length in the porous 3D *th*-B_6N_6 is 1.570 Å smaller than the 2D *th*-BN (1.583 Å),[2] as given in Table 1, confirming that 3D *th*-B_6N_6 is stronger.

3.2. Stability. We confirm the energetic stability of the 3D *th*-B_6N_6 by calculating the cohesive energy per atom (E_{coh}) as:[7]

$$E_{coh} = -\frac{E(B_6N_6) - 6E(B) - 6E(N)}{12} \quad (1)$$

where E(B), E(N), and $E(B_6N_6)$ represent the total energy of an isolated B atom, N atom, and the optimized 3D *th*-B_6N_6 compound, respectively. The computed results of E_{coh} are presented in Table 1, and the cohesive energy of porous 3D *th*-B_6N_6 (6.66 eV per atom) is found to be comparable with that of 2D tetrahexagonal BN (6.13 eV per atom);[2] however, it is lower than that of 3D wurtzite BN (8.725 eV per atom) and zinc-blende BN (8.745 eV per atom),[16] indicating its energetic stability.

Based on the following eq 2,[17,18] we further calculate the formation energy (E_f) of the 3D *th*-B_6N_6 material by using the total energies of the optimized 3D *th*-B_6N_6 compound, one B atom in the bulk alpha-B_{12} and one N atom in the alpha-N_2.

https://doi.org/10.1021/acsomega.4c06119
ACS Omega 2024, 9, 44487−44493

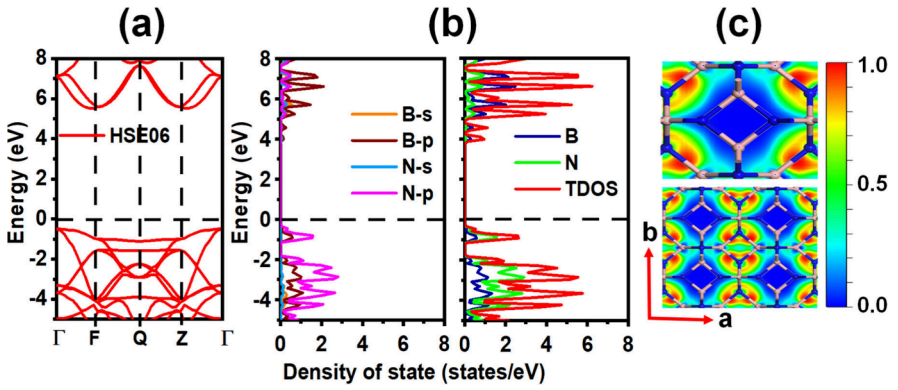

Figure 2. (a,b) Electronic band structure and density of state (PDOS and TDOS) of the 3D *th*-B_6N_6 based on the HSE06 hybrid functional. The Fermi energy level is set at 0 eV. (c) The ELF slices of the 3D *th*-B_6N_6 along the *ab*-plane estimated with GGA-PBE

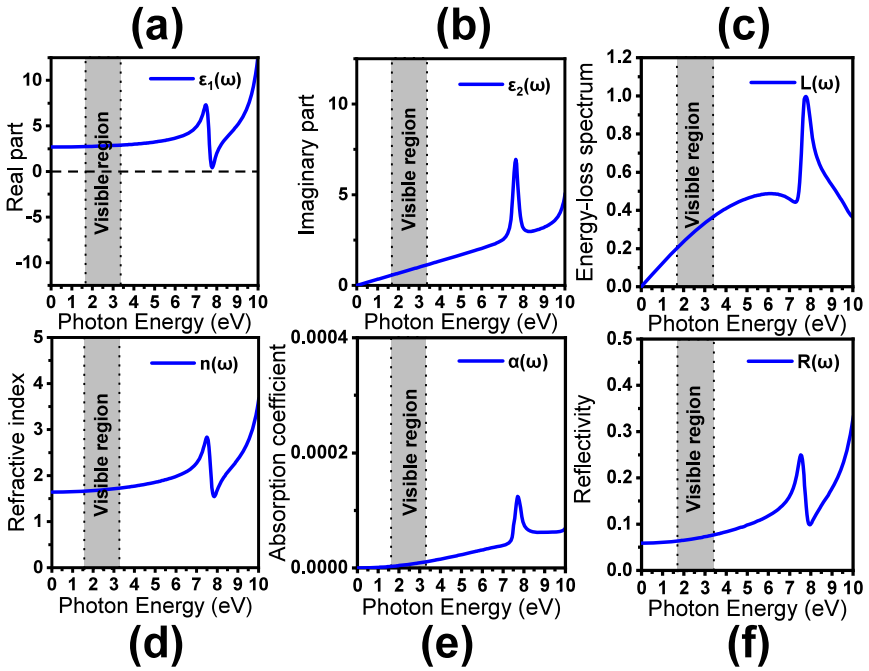

Figure 3. Computed results of the 3D *th*-B_6N_6 with HSE06 hybrid functional: (a) real and (b) imaginary parts of the dielectric function, (c) energy-loss spectrum, (d) refractive index, (e) absorption coefficient (in m^{-1}), and (f) reflectivity.

$$E_f = \frac{E(B_6N_6) - 6E(B) - 6E(N)}{12} \quad (2)$$

Therefore, the calculated value of E_f for the 3D *th*-B_6N_6 (−0.93 eV per atom) is comparable to those of the 2D *h*-BN sheet (−1.65 eV per atom) and 3D *zb*-BN (−1.50 eV per atom),[19] suggesting its synthesizability with high stability.

Furthermore, we calculate the phonon spectrum of 3D porous tetrahexagonal boron nitride to confirm the dynamic stability, and the associated result is shown in Figure 1(b). The absence of an imaginary frequency mode over the whole BZ ensures the dynamic stability of 3D *th*-B_6N_6. Also, we checked the thermal stability by conducting the AIMD simulation, and its result is presented in Figure 1(c). The total energy shows a slight variation around a constant value, and the 3D *th*-B_6N_6 structure does not show any apparent distortion simulated in the range of 300 to 700 K for 5 ps with a time step of 1 fs, indicating its thermal stability.

3.3. Electronic Properties. The reported studies show that porous boron nitrides contain wide-band-gap values. Based on the HSE06 hybrid function, we have found that 3D *th*-B_6N_6 is an excellent electrical insulator with an indirect band gap of 6.175 eV, higher than that of the 2D *th*-BN (4.49 eV)[2] (a comparison is provided in Table 1) but slightly lower than the experimental value (6.4 eV) of the 3D *zb*-BN.[21] We plot the electronic band structure and the projected and total density of states (PDOS and TDOS) in Figure 2(a,b), describing that N-p orbital electrons contribute more to the conduction band, while B-p orbital electrons share more contributions in the valence band. As the electron localization function (ELF) plays an important role in studying chemical bonding and electron distribution, we calculate the ELF in the range of 0.0−1.0, and the related results are shown in Figure 2(c). The fully localized (delocalized) electrons are stated with 1.0 (0.5), and the lowest charge density is represented with 0.0, respectively. As explained in Figure 2(c), the electrons are transferred from B to N atoms due to the electronegativity difference on the Pauling scale between the B (2.04) and N (3.04) atoms, forming strong polar covalent B−N bonds.

https://doi.org/10.1021/acsomega.4c06119
ACS Omega 2024, 9, 44487−44493

3.4. Optical Properties. Based on the calculations of the frequency-dependent dielectric function of the 3D *th*-B_6N_6, we study its optical properties (such as refractive index $n(\omega)$, energy-loss spectrum $L(\omega)$, absorption coefficient $\alpha(\omega)$ (in m^{-1}), and reflectivity $R(\omega)$). The dielectric function $\varepsilon(\omega)$ states:

$$\varepsilon(\omega) = \varepsilon_1(\omega) + i\varepsilon_2(\omega) \tag{3}$$

where the real part $\varepsilon_1(\omega)$ is associated with electronic polarizability and the imaginary part $\varepsilon_2(\omega)$ with electronic absorption, and further, they are related to the electronic band structure.[22] The Krammer−Krong relation defines the real part as:[23]

$$\varepsilon_1(\omega) = 1 + \frac{2}{\pi} P \int_0^\infty \frac{\omega' \varepsilon_2(\omega')}{\omega'^2 - \omega^2} d\omega' \tag{4}$$

where P defines the principal value. The imaginary part is given as:

$$\varepsilon_2(\omega) = \frac{2e^2\pi}{\Omega\varepsilon_0} \sum_{k,v,c} |\langle \psi_k^c | \hat{u} \times r | \psi_k^v \rangle|^2 \delta(E_k^c - E_k^v - E) \tag{5}$$

where u and e denote the incident electric field and electronic charge, and ψ_k^c and ψ_k^v represent the conduction band and valence band wave functions at wave vector k. The calculated real and imaginary parts of the dielectric function estimated with the HSE06 level are plotted in Figure 3(a,b), where the first peak of the real part occurs at 7.60 eV and specifies the excitation from the valence band maximum (VBM) to the conduction band minimum (CBM). Using the dielectric function, we also investigate $n(\omega)$, $L(\omega)$, $\alpha(\omega)$ (in m^{-1}), and $R(\omega)$:[22]

$$n(\omega) = \sqrt{\frac{|\varepsilon(\omega)| + \varepsilon_1(\omega)}{2}} \tag{6}$$

$$L(\omega) = \mathrm{Im}\left(\frac{-1}{\varepsilon(\omega)}\right) = \frac{\varepsilon_2(\omega)}{\varepsilon_1^2(\omega) + \varepsilon_2^2(\omega)} \tag{7}$$

$$\alpha(\omega) = \frac{\omega}{c}\sqrt{2(|\varepsilon(\omega)| - \varepsilon_1(\omega))} \tag{8}$$

$$R(\omega) = \left|\frac{\sqrt{\varepsilon(\omega)} - 1}{\sqrt{\varepsilon(\omega)} + 1}\right|^2 \tag{9}$$

The computed results for $L(\omega)$, $n(\omega)$, $\alpha(\omega)$, and $R(\omega)$ are displayed in Figure 3(c−f). The calculated refractive index of 3D-B_6N_6 is 1.642, and it reaches the first peak (at 2.83) in the ultraviolet (UV) region. The reflectivity value (0.072) is lower than those of other B−N systems at the PBE level, as presented in Table 2, suggesting that it can allow more light to absorb or pass through it, as compared to other BN systems. Also, the energy-loss spectrum shows a major peak in the UV region without an edge in the reflection spectra. Upon analyzing the optical absorption results of the 3D *th*-B_6N_6, it is found that absorption occurs mainly in both the visible (Vis) and UV regions within the ranges of 2.0−3.4 eV and 3.3−10 eV. Notably, this UV absorption in the 3D *th*-B_6N_6 occurs at lower energy levels when compared to BN (6.20−12.40 eV),[24] proposing the potential applications of porous 3D *th*-B_6N_6 as a good UV absorber. Moreover, a comparison with other BN-based systems is presented in Table 2, and these calculated results suggest that porous 3D *th*-B_6N_6 is an attractive candidate for optoelectronic and electrochromic applications.

Table 2. Dielectric Function $\varepsilon(\omega)$, Refractive Index $n(\omega)$, and Reflectivity $R(\omega)$ of the Porous 3D *th*-B_6N_6 as Compared with 3D *c*-BN, *h*-BN, *wz*-BN, 2D*h*-BN Sheet and 2D-BN4 Structures

Structure	Functional	$\varepsilon(\omega)$	$n(\omega)$	$R(\omega)$	Ref.
3D *th*-B_6N_6	HSE06	2.696	1.642	0.059	This work
3D *th*-B_6N_6	GGA-PBE	3.016	1.736	0.072	This work
3D*c*-BN	GGA-PBE	4.50	2.12	0.129	25
3D *h*-BN	-	3.86	1.965	0.106	26
3D *c*-BN	-	4.32	2.078	0.123	26
3D*wz*-BN	-	4.16	2.040	0.117	26
2D *h*-BN	RPA	2.09	1.44	0.033	27
2D-BN4	RPA	2.14	1.46	0.035	27

Moreover, as shown in Figure 4, we replotted Figure 3 by scaling photon energy down to the range of 0−50 meV to comprehend the property of Terahertz light absorption. It is interesting to note that a strong Terahertz light absorption can be seen in the range of 0.3−10 THz or 1.2−41.4 meV, which is comparable with the *h*-BN sheet.[4] Due to the unique cage-based configurations, chemical bonding, and wide band gap, this 3D *th*-B_6N_6 allotrope shows strong THz optical absorption. More specifically, based on the HSE06 level, the 3D *th*-B_6N_6 shows the dielectric function of 12.646, refractive index of 2.770, energy-loss spectrum of 0.977, absorption coefficient of 0.00084 (in mm^{-1}), and reflectivity of 0.3148 at 8.96 THz (37.065 meV), respectively.

3.5. Thermodynamic Properties. Furthermore, we study the thermodynamic properties such as the Debye temperature (Θ_D) and acoustic Grüneisen constant (γ_α) by using the calculated elastic constants (C_{11} = 707.76 GPa, C_{12} = 89.61 GPa, and C_{44} = 195.98 GPa), which satisfy Born−Huang criteria of the mechanical structural stability for proposed cubic symmetry of the 3D *th*-B_6N_6:[28]

$$C_{11} - C_{12} > 0, \quad C_{11} + 2C_{22} > 0, \quad C_{44} > 0 \tag{10}$$

To calculate thermodynamic properties, we have carried out calculations for mechanical properties, such as Young's modulus (E) of 558.09 GPa, shear modulus (G) of 235.40 GPa, bulk modulus (K) of 295.66 GPa, and Poisson's ratio (ν) of 0.185 based on the Voigt−Reuss−Hill approximation.[29,30] The Debye temperature describes the strength of the covalent bonds in a solid, and it can be calculated as:[31]

$$\Theta_D = \frac{h}{k_B}\left[\frac{3nN_A\rho}{4\pi M}\right]^{1/3} v_m \tag{11}$$

$$v_m = \left[\frac{1}{3}\left(\frac{2}{v_s^3} + \frac{1}{v_p^3}\right)\right]^{-1/3} \tag{12}$$

$$v_p = \left[\left(\frac{3K + 4G}{3\rho}\right)\right]^{1/2} \tag{13}$$

$$v_s = \left[\frac{G}{\rho}\right]^{1/2} \tag{14}$$

where h, n, k_B, M, N_A, and ρ denote Planck's constant, number of atoms per unit cell, Boltzmann's constant, molecular weight,

https://doi.org/10.1021/acsomega.4c06119
ACS Omega 2024, 9, 44487−44493

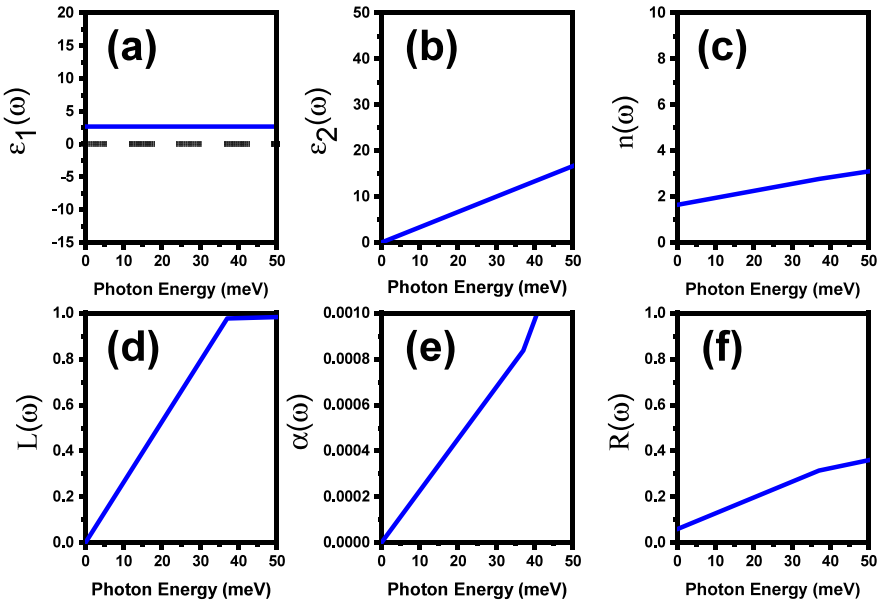

Figure 4. Computed results of the 3D *th*-B_6N_6 with HSE06 hybrid functional: (a) real and (b) imaginary parts of dielectric function, (c) refractive index, (d) energy-loss spectrum, (e) absorption coefficient (in mm^{-1}), and (f) reflectivity.

Table 3. Calculated Density ρ (in g cm^{-3}), Shear v_s, Longitudinal v_p, Mean v_m Elastic Wave Velocities (in m s^{-1}), Debye Temperature Θ_D (in K), and Acoustic Grüneisen Constant γ_α of the 3D *th*-B_6N_6 in Comparison with 3D *m*-B_5N_5 and Experimental Study of 3D Cubic BN (*c*-BN)

Structure	ρ	v_s	v_p	v_m	Θ_D	γ_α	Ref.
3D *th*-B_6N_6	2.821	9134.06	14697.96	10068.26	1304.55	1.232	This work
3D *m*-B_5N_5	3.277	10005	15293	10963	1764	1.041	20
3D *c*-BN (Exp.)	3.450	-	-	-	1625, 1700	-	32

Avogadro's number, and density, while v_m, v_p, and v_s represent the mean, longitudinal, and transverse wave velocities. The computed results for sound velocities and Debye temperature are presented in Table 3, suggesting that the Debye temperature (1304.55 K) of the 3D *th*-B_6N_6 is in good agreement with 3D *m*-B_5N_5 (1764 K)[20] and experimental values of the 3D *c*-BN (1625 K, 1700 K),[32] specifying that this structure has stronger strength of bonding.

The acoustic Grüneisen constant γ_α, which characterizes the anharmonicity between molecules or atoms in a solid, can be calculated as:[33]

$$\gamma_\alpha = \frac{3}{2}\left(\frac{3v_p^2 - 4v_s^2}{v_p^2 + 2v_s^2}\right) \quad (15)$$

where v_p and v_s denote longitudinal and transverse sound velocities, respectively. The calculated value of γ_α is 1.232, higher than the 3D *m*-B_5N_5 (1.041),[20] as presented in Table 3, describing its higher temperature or pressure dependence on this crystal's volume.

4. CONCLUSIONS

In summary, substituting C with N in the 3D-B_6C_6 results in a cage-based 3D *th*-B_6N_6 structure consisting of an excellent dynamic, thermal, and mechanical stability, along with fully sp^3-hybrid bonding. Unlike its 1D and 2D counterparts, the 3D tetrahexagonal boron nitride shows a wide band gap of 6.175 eV, exceptional Terahertz optical absorption in the range of 0.3−10 THz, Grüneisen constant of 1.232, Debye temperature of 1304.55 K, and significant phonon inelastic scattering. These exciting features, coupled with rich resources and light masses of B and N atoms, suggest that this cage-based 3D *th*-B_6N_6 is distinct from its 1D and 2D structures. Therefore, these distinctions will potentially offer promising applications in industry and technology.

■ ASSOCIATED CONTENT

Data Availability Statement

The data that support the findings of this study are available in the Supporting Information.

Supporting Information

The Supporting Information is available free of charge at https://pubs.acs.org/doi/10.1021/acsomega.4c06119.

Optimized -POSCAR.vasp of the 3D *th*-B_6N_6 structure (PDF)

■ AUTHOR INFORMATION

Corresponding Authors

Suling Shen − *Guangdong Provincial Key Laboratory of Deep Earth Sciences and Geothermal Energy Exploitation and Utilization, Institute of Deep Earth Sciences and Green Energy and Shenzhen Key Laboratory of Deep Underground Engineering Sciences and Green Energy, Shenzhen University, Shenzhen 518060, China*; Email: slshen@szu.edu.cn

Qiang Liu − *Department of Biomedical Engineering, Southern University of Science and Technology, Shenzhen 518055, China*; Email: liuq7@sustech.edu.cn

https://doi.org/10.1021/acsomega.4c06119
ACS Omega 2024, 9, 44487−44493

Authors

Kashif Hussain − *THz Technology Laboratory; Shenzhen Key Laboratory of Micro-Nano Photonic Information Technology; Key Laboratory of Optoelectronic Devices and Systems of Ministry of Education and Guangdong Province, College of Physics and Optoelectronic Engineering, Shenzhen University, Shenzhen 518060, China; School of Materials Science and Engineering, Peking University, Beijing 100871, China;* orcid.org/0000-0001-5448-3309

Muhammad Abbas − *Institute of Multidisciplinary Science, Beijing Institute of Technology, Beijing 100081, China;* orcid.org/0009-0005-2548-9425

Madhavamoorthi Suresh − *THz Technology Laboratory; Shenzhen Key Laboratory of Micro-Nano Photonic Information Technology; Key Laboratory of Optoelectronic Devices and Systems of Ministry of Education and Guangdong Province, College of Physics and Optoelectronic Engineering, Shenzhen University, Shenzhen 518060, China*

Bin Chen − *Guangdong Provincial Key Laboratory of Deep Earth Sciences and Geothermal Energy Exploitation and Utilization, Institute of Deep Earth Sciences and Green Energy and Shenzhen Key Laboratory of Deep Underground Engineering Sciences and Green Energy, Shenzhen University, Shenzhen 518060, China;* orcid.org/0000-0003-4797-7831

Ying Teng − *Guangdong Provincial Key Laboratory of Deep Earth Sciences and Geothermal Energy Exploitation and Utilization, Institute of Deep Earth Sciences and Green Energy and Shenzhen Key Laboratory of Deep Underground Engineering Sciences and Green Energy, Shenzhen University, Shenzhen 518060, China;* orcid.org/0000-0002-2323-3048

YunHong Jiang − *Guangdong Provincial Key Laboratory of Deep Earth Sciences and Geothermal Energy Exploitation and Utilization, Institute of Deep Earth Sciences and Green Energy and Shenzhen Key Laboratory of Deep Underground Engineering Sciences and Green Energy, Shenzhen University, Shenzhen 518060, China*

Qiang Sun − *School of Materials Science and Engineering, Peking University, Beijing 100871, China;* orcid.org/0000-0003-3872-7267

Zhengbiao Ouyang − *THz Technology Laboratory; Shenzhen Key Laboratory of Micro-Nano Photonic Information Technology; Key Laboratory of Optoelectronic Devices and Systems of Ministry of Education and Guangdong Province, College of Physics and Optoelectronic Engineering, Shenzhen University, Shenzhen 518060, China;* orcid.org/0000-0002-1466-7813

Complete contact information is available at: https://pubs.acs.org/10.1021/acsomega.4c06119

Notes

The authors declare no competing financial interest.

■ ACKNOWLEDGMENTS

This work is partially supported by a grant from the National Natural Science Foundation of China (No. 62205212), and Shenzhen Science and Technology Innovation Commission's Stability Support General Project (No. 20231115111049003). We thank the support from Prof. Qiang Sun and Huang Pu for giving access to computational resources (such as VASP). The calculations were supported by the High-performance Computing Platforms of both Peking and Shenzhen Universities.

■ REFERENCES

(1) Wu, H.; Xu, X.; Jiao, H.; Zhang, F.; Jia, J. Structure and Stability of Boron Nitride Cages. *Chin. Sci. Bull.* **2003**, *48* (11), 1102−1107.

(2) Kilic, M. E.; Lee, K. R. Novel Two-Dimensional Tetrahexagonal Boron Nitride with a Sizable Band Gap and a Sign-Tunable Poisson's Ratio. *Nanoscale* **2021**, *13* (20), 9303−9314.

(3) Zhang, J.; Xu, W.; Wen, H.; Cheng, X.; Zhou, S.; Li, H.; Wang, Z.; He, G. Influence of Neutron Irradiation on the Electronic Properties of Hexagonal Boron Nitride Measured by Terahertz Time-Domain Spectroscopy. *Opt. Lett.* **2023**, *48* (24), 6581.

(4) Naftaly, M.; Leist, J.; Dudley, R. Hexagonal Boron Nitride Studied by Terahertz Time-Domain Spectroscopy. *J. Phys. Conf. Ser.* **2011**, *310* (1), 012006.

(5) Zhu, L.; Borstad, G. M.; Liu, H.; Guńka, P. A.; Guerette, M.; Dolyniuk, J. A.; Meng, Y.; Greenberg, E.; Prakapenka, V. B.; Chaloux, B. L.; Epshteyn, A.; Cohen, R. E.; Strobel, T. A. Carbon-Boron Clathrates as a New Class of Sp^3-Bonded Framework Materials. *Sci. Adv.* **2020**, *6* (2), 8361.

(6) Hussain, K.; Muhammad, I.; Wu, W.; Qie, Y.; Mahmood, T.; Sun, Q. 3D Porous Metallic Boron Carbide Crystal Structure with Excellent Ductility. *Adv. Theory Simul.* **2021**, *4* (12), 2100325.

(7) Hussain, K.; Du, P. H.; Mahmood, T.; Kawazoe, Y.; Sun, Q. Three-Dimensional Tetrahexcarbon: Stability and Properties. *Mater. Today Phys.* **2022**, *23*, 100628.

(8) Kresse, G.; Furthmüller, J. Efficient Iterative Schemes for Ab Initio Total-Energy Calculations Using a Plane-Wave Basis Set. *Phys. Rev. B - Condens. Matter Mater. Phys.* **1996**, *54* (16), 11169−11186.

(9) Wende, F.; Marsman, M.; Kim, J.; Vasilev, F.; Zhao, Z.; Steinke, T. OpenMP in VASP: Threading and SIMD. *Int. J. Quantum Chem.* **2019**, *119* (12), 25851.

(10) Kresse, G.; Joubert, D. From Ultrasoft Pseudopotentials to the Projector Augmented-Wave Method. *Phys. Rev. B - Condens. Matter Mater. Phys.* **1999**, *59* (3), 1758−1775.

(11) Perdew, J. P.; Burke, K.; Ernzerhof, M. Generalized Gradient Approximation Made Simple. *Phys. Rev. Lett.* **1996**, *77* (18), 3865−3868.

(12) Heyd, J.; Scuseria, G. E.; Ernzerhof, M. Hybrid Functionals Based on a Screened Coulomb Potential. *J. Chem. Phys.* **2003**, *118* (18), 8207−8215.

(13) Monkhorst, H. J.; Pack, J. D. Special Points for Brillouin-Zone Integrations. *Phys .Rev. B - Condens. Matter Mater. Phys.* **1976**, *13* (12), 5188−5192.

(14) Togo, A.; Tanaka, I. First Principles Phonon Calculations in Materials Science. *Scr. Mater,* **2015**, *108*, 1−5.

(15) Nosé, S. A Unified Formulation of the Constant Temperature Molecular Dynamics Methods. *J. Chem. Phys.* **1984**, *81* (1), 511−519.

(16) Topsakal, M.; Aktürk, E.; Ciraci, S. First-Principles Study of Two- and One-Dimensional Honeycomb Structures of Boron Nitride. *Phys. Rev. B - Condens. Matter Mater. Phys.* **2009**, *79* (11), 15442.

(17) Hussain, K.; Muhammad, I.; Wu, W.; Qie, Y.; Mahmood, T.; Sun, Q. 3D Porous Metallic Boron Carbide Crystal Structure with Excellent Ductility. *Adv .Theory Simul.* **2021**, *4* (12), 2100325.

(18) Saha, S.; Di Cataldo, S.; Amsler, M.; Von Der Linden, W.; Boeri, L. High-Temperature Conventional Superconductivity in the Boron-Carbon System: Material Trends. *Phys. Rev. B* **2020**, *102* (2), 024519.

(19) Orellana, W.; Chacham, H. Stability of Native Defects in Hexagonal and Cubic Boron Nitride. *Phys. Rev. B Condens. Matter Mater. Phys.* **2001**, *63* (12), 1252051−1252057.

(20) Ma, Z.; Zuo, J.; Tang, C.; Wang, P.; Shi, C. Physical Properties of a Novel Phase of Boron Nitride and Its Potential Applications. *Mater. Chem. Phys.* **2020**, *252*, 123245.

(21) Furthmüller, J.; Hafner, J.; Kresse, G. Ab Initio Calculation of the Structural and Electronic Properties of Carbon and Boron Nitride Using Ultrasoft Pseudopotentials. *Phys. Rev. B -Condens. Matter Mater. Phys.* **1994**, *50* (21), 15606−15622.

(22) Hussain, K.; Younis, U.; Muhammad, I.; Qie, Y.; Guo, Y.; Li, T.; Xie, H.; Sun, Q. Three-Dimensional Porous Borocarbonitride BC_2N with Negative Poisson's Ratio. *J. Mater. Chem. C Mater* **2020**, *8* (44), 15771−15777.
(23) Gajdoš, M.; Hummer, K.; Kresse, G.; Furthmüller, J.; Bechstedt, F. Linear Optical Properties in the Projector-Augmented Wave Methodology. *Phys. Rev. B - Condens. Matter Mater. Phys.* **2006**, *73*, 045112.
(24) Sun, C.; Ma, F.; Cai, L.; Wang, A.; Wu, Y.; Zhao, M.; Yan, W.; Hao, X. Metal-Free Ternary BCN Nanosheets with Synergetic Effect of Band Gap Engineering and Magnetic Properties. *Sci. Rep.* **2017**, *7* (1), 1−8.
(25) Sun, J.; Zhou, X. F.; Fan, Y. X.; Chen, J.; Wang, H. T.; Guo, X.; He, J.; Tian, Y. First-Principles Study of Electronic Structure and Optical Properties of Heterodiamond BC_2N. *Phys. Rev. B - Condens. Matter Mater. Phys.* **2006**, *73* (4), 045108.
(26) Xu, Y. N.; Ching, W. Y. Calculation of Ground-State and Optical Properties of Boron Nitrides in the Hexagonal, Cubic, and Wurtzite Structures. *Phys. Rev. B* **1991**, *44* (15), 7787−7798.
(27) Shahrokhi, M.; Mortazavi, B.; Berdiyorov, G. R. New Two-Dimensional Boron Nitride Allotropes with Attractive Electronic and Optical Properties. *Solid State Commun.* **2017**, *253*, 51−56.
(28) Mouhat, F.; Coudert, F. X. Necessary and Sufficient Elastic Stability Conditions in Various Crystal Systems. *Phys. Rev. B - Condens. Matter Mater. Phys.* **2014**, *90* (22), 054115.
(29) Hill, R. The Elastic Behaviour of a Crystalline Aggregate. *Proc. Phys.Soc. A* **1952**, *65* (5), 349−354.
(30) Chung, D. H.; Buessem, W. R. The Voigt-Reuss-Hill Approximation and Elastic Moduli of Polycrystalline MgO, CaF_2, *β*-ZnS, ZnSe, and CdTe. *J. Appl. Phys.* **1967**, *38* (6), 2535−2540.
(31) Anderson, O. L. A Simplified Method for Calculating the Debye Temperature from Elastic Constants. *J. Phys. Chem. Solids* **1963**, *24* (7), 909−917.
(32) Vel, L.; Demazeau, G.; Etourneau, J. Cubic Boron Nitride: Synthesis, Physicochemical Properties and Applications. *Mater. Sci. Eng. B* **1991**, *10* (2), 149−164.
(33) Han, W. D.; Li, K.; Dai, J.; Li, Y. H.; Li, X. Du. Structural, Mechanical, and Thermodynamic Properties of Newly-Designed Superhard Carbon Materials in Different Crystal Structures: A First-Principles Calculation. *Comput. Mater. Sci.* **2020**, *171*, 109229.

https://doi.org/10.1021/acsomega.4c06119
ACS Omega 2024, 9, 44487−44493